

Equations of State, Thermodynamics, and Miscibility Curves for Jovian Planet and Giant Exoplanet Evolutionary Models

ROBERTO TEJADA AREVALO ,¹ YUBO SU ,¹ ANKAN SUR ,¹ AND ADAM BURROWS ,¹

¹*Department of Astrophysical Sciences, Princeton University, 4 Ivy Ln, Princeton, NJ 08544, USA*

ABSTRACT

The equation of state of hydrogen-helium (H-He) mixtures plays a vital role in the evolution and structure of gas giant planets and exoplanets. Recent equations of state that account for hydrogen-helium interactions, coupled with hydrogen-helium immiscibility curves, can now produce more physical evolutionary models, such as accounting for helium rain with greater fidelity than in the past. In this work, we present a set of tools for planetary evolution^{a)} that provides a Python interface for tables of useful thermodynamic quantities, state-of-the-art H-He equations of state, and pressure-dependent immiscibility curves. In particular, for a collection of independent variable choices, we provide scripts to calculate a variety of thermodynamic derivatives used to model convection and energy transport. This centralized resource is meant to facilitate and consolidate giant planet structural and evolutionary modeling going forward.

Keywords: Chemical thermodynamics, Planetary interiors, Solar system giant planets, Extrasolar gaseous giant planets

1. INTRODUCTION

The structure and evolution of gas giant planets and brown dwarfs depend on the properties of hydrogen and helium at high pressures (Hubbard 1970; Hubbard & Slattery 1971; Hubbard & DeWitt 1985; Burrows et al. 1997, 2001; Fortney & Hubbard 2003, 2004; Militzer et al. 2008; Nettelmann et al. 2008, 2012, 2015; Hubbard & Militzer 2016; Mankovich et al. 2016; Püstow et al. 2016; Miguel et al. 2016; Debras & Chabrier 2019; Mankovich & Fortney 2020; Debras et al. 2021a; Mankovich & Fuller 2021; Howard et al. 2023), as well as their atmospheres (Burrows et al. 1997; Fortney et al. 2011; Burrows 2014; Chen et al. 2023). The equation of state (EOS) most employed in the past was published by Saumon et al. (1995, SCvH95). This EOS incorporated the so-called “chemical picture” of the constituent species, obtained by minimizing the Helmholtz free energy of its constituents. This model estimated a gradual disassociation and ionization of hydrogen with increasing pressure, thus accounting for the increasing densities and even the predicted hydrogen first-order phase transition within Jupiter. Subsequent ab initio calculations by Militzer & Hubbard (2013, MH13) and Nettelmann et al. (2012), which included non-ideal interaction effects of hydrogen-helium mixtures and partial ionizations, were an important step forward. Models using updated EOSes by MH13 and Nettelmann et al. (2012) and the SCvH95 EOS resulted in significant differences in the interior structures of Jupiter and Saturn (see Miguel et al. 2016; Militzer & Hubbard 2013; Hubbard & Militzer 2016; Miguel et al. 2022). Further complications arose when applying such EOSes to such modeling due to 1) the phase separation of helium related to the metallization of hydrogen at high pressures; 2) the presence of a higher-Z core; and 3) the presence of a component of heavy elements in the gaseous mantle. The distribution of the latter is the subject of intense debate following the recent interpretations (Leconte & Chabrier 2012, 2013; Vazan et al. 2016; Wahl et al. 2017; Folkner et al. 2017; Vazan et al. 2018; Stevenson 2020; Helled et al. 2022; Militzer et al. 2022; Howard et al. 2023) of the *Juno* (Bolton et al. 2017a,b) gravity data. To this end, two primary areas of focus are an improved H-He EOS and a more accurate H-He phase separation curve.

The first area, the H-He EOS, demands ab initio calculations of relevant thermodynamic quantities. The computational costs have impeded the creation of a comprehensive tabular EOS for a wide range of hydrogen-helium mixtures, temperatures, and pressures. As a re-

^{a)} Available at https://github.com/Rob685/hhe_eos_misc

sult, current EOSes employed in structural and evolutionary codes, such as those of SCvH95, (Nettelmann et al. 2012; Becker et al. 2013), Chabrier et al. (2019, CMS19) and Mazeved et al. (2022, MLS22), rely on idealized mixing laws to compute the entropy of H-He mixtures. However, a newer class of models includes non-ideal effects of the entropy of mixing. These terms have recently been estimated by Howard & Guillot (2023, HG23) based on the calculations of MH13, who calculated a H-He mixture EOS for a helium mass fraction (Y) of 0.245. This resulted in estimates for the non-ideal corrections for any helium mass fraction for the CMS19 and MLS22 EOSes.

In the second area, the H-He phase separation curves, Lorenzen et al. (2009, 2011), Morales et al. (2013), and Schöttler & Redmer (2018) have employed ab initio techniques to determine the phase separation curves of hydrogen and helium mixtures. On the experimental front, Brygoo et al. (2021) conducted cutting-edge experiments on H-He phase separation and found significant disagreements with the ab initio calculations. Moreover, those ab initio calculations are not accompanied by corresponding EOSes, and the CMS19 and MLS22 EOSes are not accompanied by miscibility curves. Therefore, the predominant hybrid approach used in planetary evolution calculations, combining EOSes and phase separation curves from different studies, is inconsistent. However, the utility of this approach cannot be denied, and the ease of use of both EOSes and miscibility curves is of great importance.

Between the different EOS and phase separation calculations by various authors, planetary modelers have a wide range of options. In this paper, we collect many major EOS and miscibility databases required for giant planet evolutionary and structural calculations and describe their strengths and weaknesses¹. We invert each EOS on a dense grid and calculate all the necessary quantities and derivatives that play a role in the physics, structure, thermal evolution, and convection criteria within Jupiter and Saturn in particular, and giant exoplanets in general. Each EOS is calculated along pressure-temperature, density-temperature, and entropy-density axes that span the thermodynamic range of the interiors of gas giants. As discussed in Section 5, a proper treatment of convection requires

the calculation of various derivatives. In addition to the various EOS tables, we furnish useful tables of the hydrogen-helium immiscibility curves of Lorenzen et al. (2009, 2011) and Schöttler & Redmer (2018). In this way, our work provides a more centralized and standardized approach by collecting the most recent EOS and H-He immiscibility data in a self-consistent format.

This paper is organized as follows. Section 2 discusses the various hydrogen-helium (H-He) EOSes, compares their properties, and discusses their applications. In Section 3, we provide an overview of the available miscibility calculations in the literature, compare the different demixing temperature calculations of each of the sources, and discuss their differences vis à vis planetary evolution. In Section 4, we briefly discuss the thermodynamic consistency of the EOSes published by Saumon et al. (1995) and Chabrier et al. (2019). In Section 5, we discuss the various derivatives necessary for generalized convection and we review the different derivatives necessary for energy calculations in a planetary model. Finally, in Section 6, we provide a summary discussion and concluding remarks. In the appendices, we derive various of the relationships provided in the text.

2. HYDROGEN AND HELIUM EQUATIONS OF STATE

Historically, the EOS of hydrogen and helium at high pressures has been divided into the “physical” picture and the “chemical” picture. In the physical picture, electrons and nuclei interact through Coulomb potentials, and the EOS is obtained by solving the resulting quantum many-body problem. In the chemical picture, atoms remain bound and interact through pair potentials. However, at ionization pressures and temperatures, electrons become unbound and delocalized. In the high temperature regime, electrons become unbound and the physical picture is tractable (Rogers 1981; Rogers & Young 1984), and interactions under the Thomas-Fermi approach (Myers & Swiatecki 1990, 1996). However, in the low-temperature and high-pressure regime relevant to gas giant planets, the physical picture remained intractable due to partial ionization. The chemical picture presents a simplified model a physical model. In the past, the chemical picture model of SCvH95 was the most commonly used H-He EOS. However, with improvements in computation, rigorous physical (or “ab initio”) models have been published. Most notably, MH13, CMS19, Chabrier & Debras (2021, CD21), and MLS22 have published EOSes obtained from ab initio calculations. As discussed in the introduction, these previous EOSes handle arbitrary H-He mixtures via the ideal additive volume law (AVL;

¹ We omit the H-He EOS of Nettelmann et al. (2012) and Becker et al. (2014) due to the lack of entropy calculations available in their tables. An integration technique to obtain the entropy for these tables depends on choices of initial thermodynamic values, making the comparisons between EOSes uncertain and subsequent derivative calculations subject to this uncertainty.

see Section 2.1). This approximation was improved by HG23, who have calculated nonideal interaction corrections based on the MH13 results for the CMS19 and MLS22 EOSes. In this section, we discuss the properties of the historical SCvH95, the ab initio MH13, and the most current CMS19 EOSes and compare their properties².

2.1. Saumon, Chabrier, and van Horn (1995)

Saumon et al. (1995, SCvH95) employed the chemical picture and generated an EOS that covered a temperature range of $2.10 \leq \log_{10} T [K] \leq 7.06$ and a density range of $-6.00 \leq \log_{10} \rho [g \text{ cm}^{-3}] \leq 3.75$. They calculated pure hydrogen and helium tables and relied on the additive-volume law (AVL), also referred to as the “volume-addition law,” to handle a general helium mass fraction dependence. Intensive variables, such as temperature and pressure, must be uniform throughout a system at equilibrium. Extensive variables, such as volume and entropy, are additive for a system in equilibrium. Therefore, the AVL considers a combined system of equations of state and assumes they are in thermal and pressure equilibrium. AVL cannot account for interactions between hydrogen and helium, is not reliable in regions of partial ionization, and it does not account for phase separation (see Section 6 of SCvH95 for more detailed descriptions of its limitations). Despite these limitations, until recently, SCvH95 was the most used EOS in the study of low-mass stars, brown dwarfs, and giant planets (e.g., Burrows et al. 1995; Guillot et al. 1996; Saumon et al. 1996; Burrows et al. 1997; Chabrier & Baraffe 1997; Baraffe et al. 1998; Burrows et al. 2001; Fortney & Hubbard 2003, 2004; Fortney et al. 2011)

The additive volume law states that

$$\frac{1}{\rho(P, T)} = \frac{1 - Y}{\rho_H(P, T)} + \frac{Y}{\rho_{He}(P, T)}, \quad (1)$$

where ρ_H , ρ_{He} , and ρ are the mass densities of hydrogen, helium and mixtures, respectively, at constant pressure and temperature. This corresponds to

$$s(P, T) = s_H(P, T)(1 - Y) + s_{He}(P, T)Y + s_{id}, \quad (2)$$

where s_H , s_{He} , and s_{id} are the hydrogen, helium, and the ideal entropy of mixing, respectively. The SCvH95 EOS estimated entropy of mixing for each component i

² The MLS22 EOS result is a hydrogen EOS table benchmarked with structural calculations of the interior of Jupiter inferred from the *Juno* data. Though we present this EOS and provide the same quantities and derivatives for it, we focus here on the CMS19 and SCvH95 EOSes.

of m systems,

$$s_{id} = k_b \left[N \ln N - \sum_{i=1}^m N_i \ln N_i \right]. \quad (3)$$

This generalizes to all ionization states in their EOS and was used to compute the ideal entropy of mixing for H-He mixtures (see equations 53–56 in SCvH95).

The SCvH95 EOS conveniently provides many of these derivatives, making it the standard for H-He EOSes in the warm-dense region of planetary interiors and low mass stars (Burrows et al. 1997, 2001). For all its strengths, the most challenging region for the SCvH95 EOS is that of partial ionization in the region of ~ 1 Mbar, which is relevant for gas giant interiors. The limits of the chemical paradigm, such as the ionization states of different chemical species, are overcome by ab initio simulations under the physical picture.

2.2. Militzer & Hubbard (2013)

The Militzer & Hubbard (2013, MH13) EOS spans a temperature range of $500 \leq T \leq 120,000$ K and a density range of $0.1 \leq \rho \leq 6 \text{ g cm}^{-3}$. As their model is a physical model, they avoid the limitations of the low-temperature and high-pressure regime inherent in the chemical model of SCvH95. They use Density Functional Theory Molecular Dynamics (DFT-MD), coupled with the thermodynamic integration (TDI) technique, to obtain the entropy directly through the difference in Helmholtz free energy between hydrogen and helium mixtures. To account for interactions between species and electrons, they used intramolecular pair potentials derived at a particular density and temperature and the Perdew-Burke-Ernzerhof (Perdew et al. 1996, PBE) exchange-correlation functional.

Since MH13 calculated their ab initio EOS only for $Y = 0.245$, they used the AVL for arbitrary mixtures. Since the AVL requires another helium fraction, the $Y = 0.245$ EOS table can be combined with an ab initio helium EOS calculated by Militzer (2009). In principle any helium EOS can be used (e.g., see Miguel et al. 2016, who used the SCvH95 helium EOS). The AVL can be adjusted to interpolate between any given H-He mixture, Y_1 and Y_2 , by

$$\frac{1}{\rho} = \frac{Y - Y_1}{Y_2 - Y_1} \frac{1}{\rho_2} + \frac{Y_2 - Y}{Y_2 - Y_1} \frac{1}{\rho_1}, \quad (4)$$

where $Y_1 \leq Y \leq Y_2$, ρ_1 and ρ_2 are the densities at Y_1 and Y_2 respectively. For a pure helium EOS and a mixture EOS, Equation 4 reduces to Equation 3 of Hubbard & Militzer (2016).

The MH13 EOS addressed many of the shortcomings of the SCvH95 EOS, but its lack of coverage in the shallow interior ($\lesssim 0.1$ Mbar) prompted the use of other

EOS prescriptions in such regions. To overcome these obstacles, recent work (see [Mankovich & Fuller 2021](#), for example) uses a combination of EOS tables, including that of MH13, for better coverage in the density, temperature, and pressure space and greater flexibility with helium fraction dependencies. Next, we discuss the most recent work by CMS19 and CD21 to obtain a comprehensive H-He EOS.

2.3. Chabrier, Mazeret, and Soubiran (2019)

[Chabrier et al. \(2019\)](#), CMS19 constructed pure hydrogen and helium EOS tables spanning wider density and temperature ranges, namely $10^{-8} \leq \rho \leq 10^6 \text{ g cm}^{-3}$ and $100 \leq T \leq 10^8 \text{ K}$. For densities lower than 0.05 g cm^{-3} , they use the SCvH95 hydrogen EOS, the hydrogen EOS of [Caillabet et al. \(2011\)](#) for $0.3 \leq \rho \leq 5.0 \text{ g cm}^{-3}$, and the EOS of [Chabrier & Potekhin \(1998\)](#) for densities greater than 10 g cm^{-3} .

As SCvH95, their EOS rely on the AVL for helium mixtures and include only the ideal entropy of mixing. CD21 attempted to incorporate the non-ideal interaction effects of MH13 into the CMS19 EOS using methods from [Miguel et al. \(2016\)](#). Using the AVL, they obtained an “effective” hydrogen EOS from MH13 using the CMS19 helium EOS to obtain a mixture for $Y = 0.275$. With this correction, the CD21 results agree at higher densities with MH13 (see Figure 9 of CD21).

To further address this shortcoming, [Howard & Guillot \(2023\)](#), HG23 extended the interaction correction to arbitrary Y by prescribing a non-ideal correction term of form

$$s = s_{\text{H}}(1 - Y) + S_{\text{He}}Y + Y(1 - Y)\Delta S_{XY}, \quad (5)$$

$$\frac{1}{\rho} = \frac{1 - Y}{\rho_{\text{H}}} + \frac{Y}{\rho_{\text{He}}} + Y(1 - Y)\Delta V_{XY}, \quad (6)$$

and requiring that these corrections agree with MH13 at $Y = 0.245$ and with CD at $Y = 0.275$. The corrections, ΔS_{XY} and ΔV_{XY} , are assumed to be proportional to the products of hydrogen and helium mass fractions.

The CMS19 EOS with the HG23 corrections (CMS19+HG23) is the most current development of an H-He EOS that spans all relevant thermodynamic space, helium fractions, and nonideal interactions. Based on this, we advocate CMS19 + HG23 EOS as a current default baseline. In Figure 1, we compare the CMS19+HG13 and MLS22+HG23 EOSes with the SCvH95, MH13, CMS19, and CD21 tables, illustrating the differences among them. The top panel mirrors Figure 4 of HG23, comparing the EOSes at a helium fraction of $Y = 0.245$ and a specific entropy of

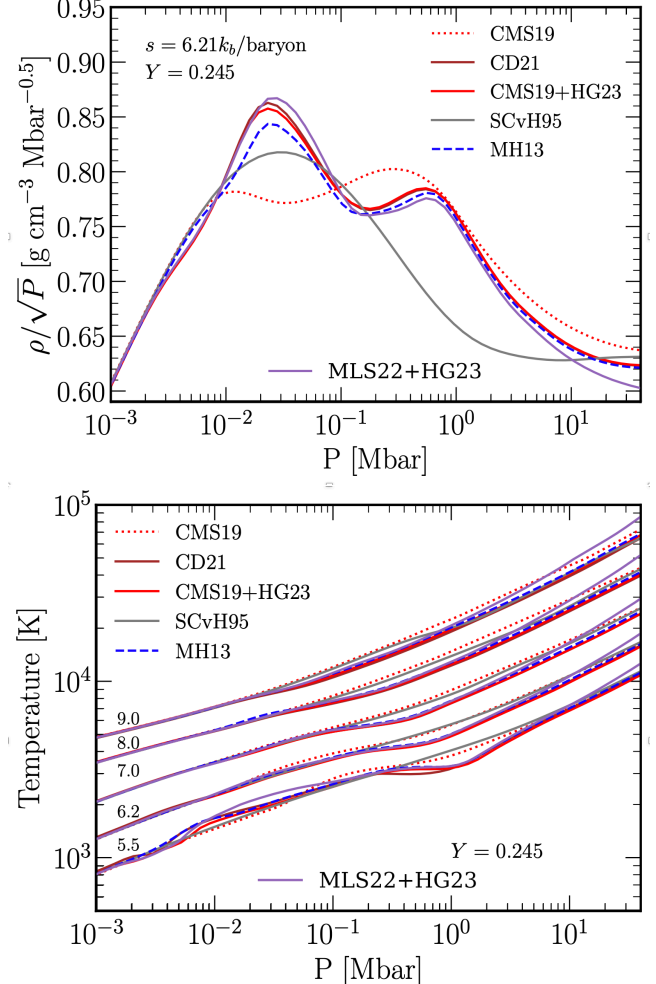


Figure 1. Top: Reproduction of Figure 4 of [Howard & Guillot \(2023\)](#) with corresponding labels for $Y = 0.245$ and $s = 6.21 k_b \text{ baryon}^{-1}$. Bottom: Adiabatic profiles at different entropy values in $k_b \text{ baryon}^{-1}$ units. We replicate the behavior shown in Figure 10 of [Militzer & Hubbard \(2013\)](#); at modest pressures of $\sim 1 \text{ Mbar}$, the non-ideal effects cause the equations of state to deviate from SCvH95. The region where the SCvH95 deviates significantly is the same region where hydrogen and helium are expected to demix.

$s = 6.21 k_b/\text{baryon}$. The bottom panel shows the temperature differences due to the non-ideal interactions at different entropy values, as noted above, for each profile. The density deviations from SCvH95 increase with decreasing entropy, particularly between 0.5 and 7 Mbar. This pressure region is expected to exhibit H-He phase separation at a sufficiently low temperature ([Stevenson 1975](#); [Stevenson & Salpeter 1977](#)). In the next section, we discuss the current understanding of H-He immiscibility in this context.

3. HYDROGEN AND HELIUM IMMISCIBILITY

Early evolutionary calculations for Saturn (Pollack & Graboske 1976; Pollack et al. 1977) could not reproduce its current heat flux. To account for this apparent excess heat, Stevenson (1975) proposed the formation of He-rich droplets that rain into the interior (also see Stevenson & Salpeter 1977). One of the first attempts to capture and apply the demixing of hydrogen and helium as a function of helium abundance was done by Hubbard & Dewitt (1985), who applied Monte Carlo simulations for a fully ionized hydrogen and helium plasma. The low-pressure regime was studied by Schouten et al. (1991) via Monte Carlo methods using pair potentials for interactions. Pfaffenzeller et al. (1995) calculated the demixing temperatures using molecular dynamics (MD) and found a demixing temperature-pressure dependence opposite that of Hubbard & Dewitt (1985). However, the demixing temperatures remained too cold for Saturn to ever reach the immiscibility regions (Pfaffenzeller et al. 1995; Fortney & Hubbard 2003). Fortney & Hubbard (2003) created an ad hoc phase diagram, adjusting the demixing temperatures of Pfaffenzeller et al. (1995), to match the present effective temperature of Saturn. More recently, H-He phase diagrams have been calculated by Lorenzen et al. (2009, 2011, L0911), Morales et al. (2009, 2013), and Schöttler & Redmer (2018, SR18). These ab initio phase diagrams are discussed in the next sections.

3.1. Lorenzen et al. (2009, 2011)

Lorenzen et al. (2009, L0911) conducted the first ab initio immiscibility gap model. They used DFT coupled with Car-Parrinello MD, which was also used by Pfaffenzeller et al. (1995), with a PBE exchange-correlation functional and pair potentials for hydrogen and helium. They calculated the demixing temperatures for pressures between 4 Mbar and 24 Mbar and expanded their model in Lorenzen et al. (2011) to include 1 and 2 Mbar. In all cases, they relied on linear mixing to calculate the enthalpy of mixing to then infer the change in the Gibbs free energy, G . This was then minimized to constrain the H-He miscibility gaps. They linearized the change in the enthalpy with

$$\Delta H(x) = H(x) - xH(1) - (1 - x)H(0), \quad (7)$$

where x is the number fraction of helium. They used the relation,

$$\Delta G(x) = \Delta H(x) - T\Delta S_{\text{id}}, \quad (8)$$

where $\Delta S_{\text{id}} = -k_b[x \log x + (1 - x) \log(1 - x)]$ is the change in the ideal entropy of mixing. This term does not account for any non-ideal interactions in their EOS.

With a helium abundance-dependent phase diagram, one can interpolate between the isobars and invert it to

yield the demixing temperature profiles. The right panel of Figure 2 shows the helium dependence of the demixing temperatures for each isobar calculated by L0911. Temperatures below each of these lines indicate regions where the hydrogen and helium phase separate. In Figure 3, the SCvH95 (solid lines) and CMS19+HG23 (dotted lines) temperature profiles are calculated for a constant helium fraction of $Y = 0.27$ and a specific entropy of $s = 6.21 k_b/\text{baryon}$, believed to be the present-day entropy of an adiabatic Jupiter as inferred by the Galileo probe entry (Seiff et al. 1997, 1998). The bottom panel shows the demixing profiles of L0911. For example, since both EOS profiles intercept the $Y = 0.27$ demixing curve (in red), it is expected that demixing occurs between 1 Mbar and 2 Mbar for SCvH and 1 Mbar and 5 Mbar for the CMS19+HG3 temperature profile.

The phase diagrams from L0911 predict a large miscibility gap in Saturn (Püstow et al. 2016) and little to no gap in Jupiter (Mankovich et al. 2016) at the present age. Püstow et al. (2016) claim that the L0911 diagrams need corrections of -1300 K and 500 K for Jupiter and Saturn, respectively. In the next section, we discuss the work of Morales et al. (2009, 2013) and their inclusion of non-ideal interactions in the phase diagram.

3.2. Morales et al. (2009, 2013)

Morales et al. (2009) constructed the first H-He phase diagram that included non-ideal interaction effects in the entropy of mixing, following a similar methodology to that of Militzer (2009) and MH13. Instead of the Car-Parrinello MD, Morales et al. (2009) used the Born-Oppenheimer MD coupled with the PBE exchange-correlation functional, and used TDI to infer the entropy using the Helmholtz free energy difference (also used by MH13). Morales et al. (2013) expanded their work to pressures below 0.4 Mbar, and claimed that the linear mixing assumption leads to significant disagreements with their direct calculation methods at high helium mass fractions and high pressures.

This work led to colder demixing temperatures compared to L0911. While Jupiter had a small miscibility gap between ~ 1 Mbar and ~ 3 Mbar with the L0911 phase diagram, the Morales demixing temperature results were too cold to allow Jupiter any miscibility gap (Morales et al. 2013). For consistency, Hubbard & Militzer (2016) used the Morales phase diagram, since both the EOS and the demixing temperatures were calculated in a similar fashion. Hubbard & Militzer (2016) then claimed that helium rain occurs within Jupiter at an entropy value of $s \approx 6 k_b/\text{baryon}$. However, as Mankovich et al. (2016) and Mankovich & Fortney (2020) also discuss, Morales temperatures were only calculated for a

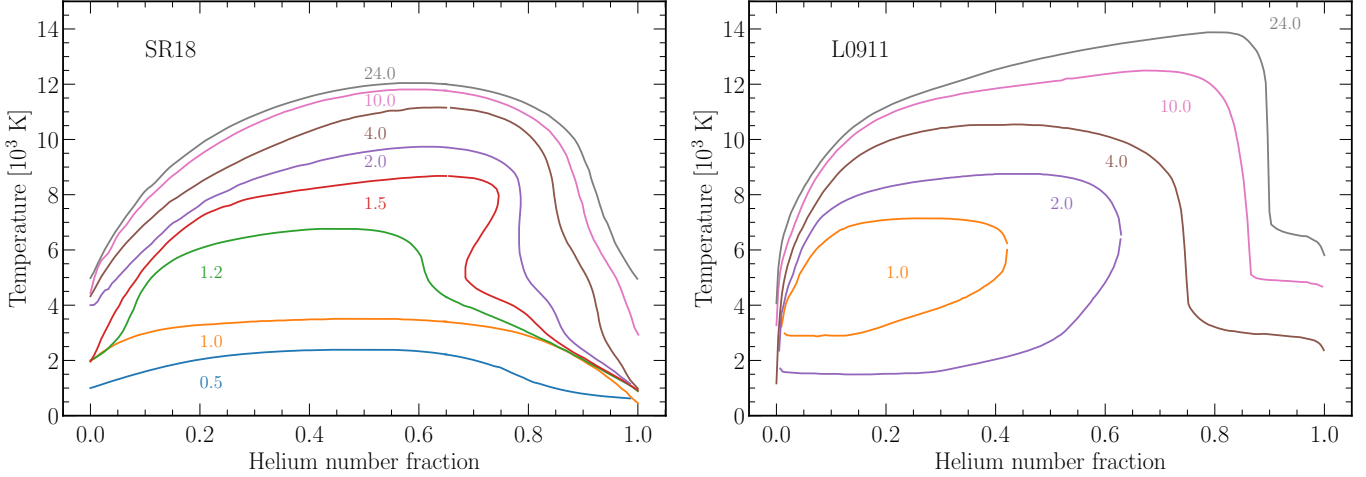


Figure 2. Differences in demixing temperature calculations as a function of helium abundance. Left: Schöttler & Redmer (2018, SR18), using van der Waals exchange-correlation functional including nonideal effects on the entropy and Right: Lorenzen et al. (2009, 2011, L0911), using the PBE exchange-correlation functional and the linear mixing rule. Using the van der Waals functional and including the non-ideal effects for the entropy leads to colder demixing temperatures, particularly at low pressures. The regions under each curve are immiscibility regions of hydrogen and helium. These authors calculated such curves for constant pressures, all of which are highlighted by color here, in Mbar.

fraction of helium of $x_{\text{He}} = 0.08$. Given that helium is expected to redistribute inside any gas giant planet, a faithful model of the interiors of these planets that takes into account helium rain must be a function of helium abundance. In the following section, we discuss the work of Schöttler & Redmer (2018), which used ab initio methods, including non-ideal effects, but also as a function of helium abundance.

3.3. Schöttler & Redmer (2018)

Schöttler & Redmer (2018, SR18) performed ab initio simulations using a van der Waals exchange-correlation functional instead of PBE, claiming that their method better captured the Gibbs free energy compared to previously used methods. By calculating the non-ideal effects in the entropy, SR18 calculated the demixing temperatures shown on the left panel of Figure 2. It is clear that each isobar from SR18 is significantly colder than those of L0911. The 1 Mbar demixing region is significantly smaller for the van der Waals DFT result. Qualitatively, whereas L0911 showed enclosed regions of miscibility at low pressures, SR18 show flat and open regions at those pressures, leading to even colder demixing temperatures. The top panel of Figure 3 shows the demixing temperature profiles with colors corresponding to those of L0911 in the bottom panel. Note that for very low helium number fractions, the temperatures are comparable, but remain significantly lower for higher helium abundances.

When the demixing profiles are compared in the abundance of $Y = 0.27$, the abundance for which Morales cal-

culated their miscibility curves, the L0911 and Morales curves are hotter than the SR18 profiles by ~ 1000 and ~ 500 K, respectively. Figure 4 shows these profiles (colored lines) compared to adiabats for the SCvH95 and CMS19+HG23 equations of state. If the demixing temperatures of SR18 are used to determine miscibility gaps in gas giant planets, then these will lead to narrower H-He immiscibility regions compared to L0911. The bottom panel of Figure 4 shows decreasing entropy adiabats for both EOSes. Once the adiabat intercepts the miscibility curve, the regions highlighted in red undergo H-He phase separation. For a constant helium fraction of $Y = 0.27$, this occurs at $s = 6.0$ k_b/baryon for the CMS19+HG23 EOS and roughly at $s = 5.8$ k_b/baryon for the SCvH EOS. We show the L0911 and SR18 miscibility gaps as a function of entropy and helium mass fraction in Figure 5. The gaps grow as entropy and helium mass fraction decrease. As helium mass fraction increases, immiscibility regions open only at lower entropies. Figure 5 illustrates the difference of each miscibility diagram, where L0911 can achieve miscibility gaps at higher entropies than SR18. Since the SR18 curves are significantly cooler, they require lower entropies. Because of this, Mankovich & Fortney (2020) claimed that if helium rain is responsible for the excess heat of Saturn, the demixing temperatures need to be hotter by ~ 540 K. Recently, Brygoo et al. (2021) empirically measured a miscibility curve for $Y = 0.33$, highlighted in red in the top panel of Figure 4. While they found a positive upward shift in the temperature from the SR18 curve,

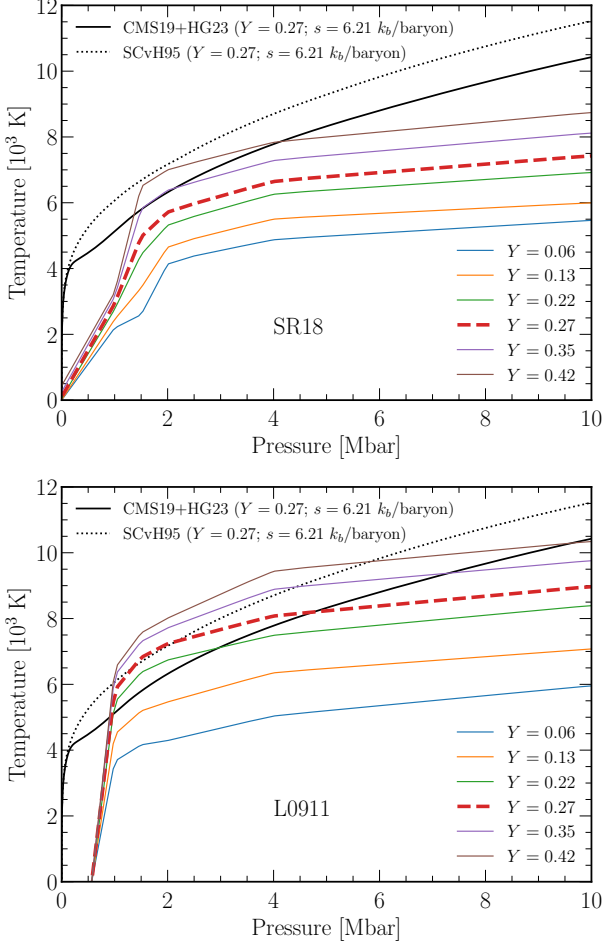


Figure 3. H-He miscibility curves for various Helium fractions with SCvH95 and CMS19+HG23 adiabats at $s = 6.1 \text{ } k_b/\text{baryon}$ and at a constant $Y = 0.27$. The profiles would experience H-He demixing when they osculate the $Y = 0.27$ curve, which is highlighted as the dashed red line. The top panel shows curves of constant helium abundance for the SR18 data and the bottom for the L0911 data. The SR18 $Y = 0.27$ curve is too cold for any of the adiabats to cross it. The L0911 $Y = 0.27$ is hot enough to allow each adiabat a miscibility region.

the shift is $\sim 2,000 \text{ K}$, which is far larger than the shift predicted by Mankovich & Fortney (2020).

The SR18 H-He miscibility data have several advantages over the L0911 and Morales data. Its advantage over the L0911 phase diagram is its inclusion of non-ideal entropy of mixing, while both the SR18 and L0911 data have an advantage over the Morales phase diagram in its provision of remixing temperatures for an arbitrary helium mass fraction. Based on this history and due to their inclusion of a dependence on the helium mass fraction, we advocate in the near term the use of the L0911 and SR18 curves as the best current options. However, we note that temperature shifts in these curves to

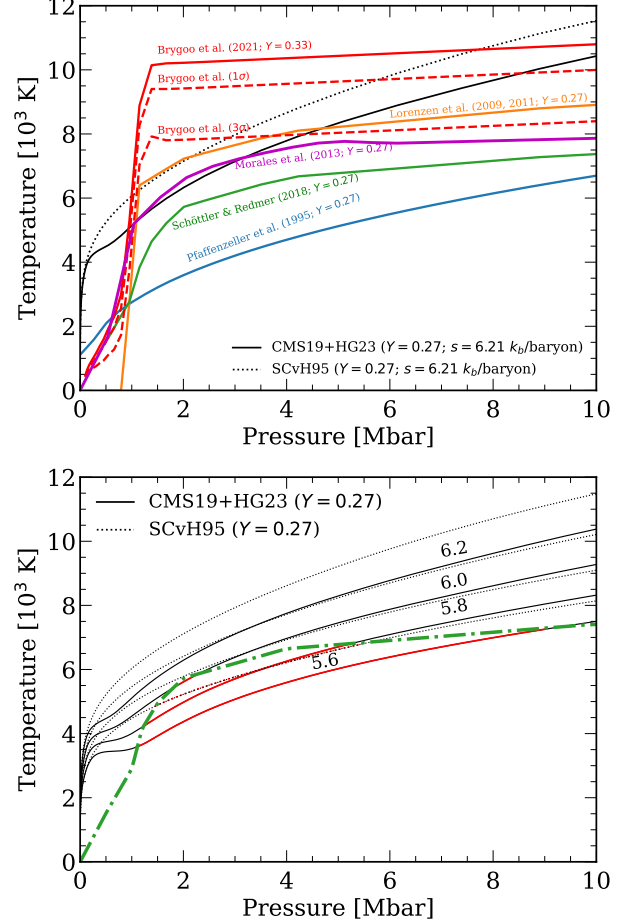


Figure 4. Top: Miscibility curves from Lorenzen et al. (2009, 2011); Morales et al. (2013); Schöttler & Redmer (2018), with the parametrization of Pfaffensteller et al. (1995) from Fortney & Hubbard (2003) at constant helium abundance ($Y = 0.27$). The EOS adiabats are also at $Y = 0.27$ and fixed at a constant specific entropy of $s = 6.21 \text{ } k_b/\text{baryon}$. The SR18 curve is highlighted as the green dashed curve, since it represents the latest development in H-He miscibility. The Bryggo et al. (2021) experimental curve is plotted to compare with the others, but it was measured for the helium abundance of $Y = 0.33$. Included are also the (minus) 1σ and 3σ error lines for the Bryggo et al. (2021) data. The SR18 curve remains at $Y = 0.27$ and EOS adiabats are plotted for a range of entropy values in units of k_b/baryon . Once the profiles intercept the miscibility curve, the pressure regions highlighted in red will experience H-He phase separation. As entropy decreases, the miscibility gap expands to cover a wider pressure region.

alter their demixing temperatures still seem necessary. Such temperature changes echo the suggestions of Nettelmann et al. (2015), Püstow et al. (2016), Mankovich et al. (2016), and Mankovich & Fortney (2020).

We make the L0911 and SR18 immiscibility curves accessible and provide prescriptions to use for giant planet

evolutionary and structural calculations. These H-He miscibility prescriptions are allowed to follow the pressure, temperature, and helium abundance of a given planetary interior profile. Therefore, these adapt to the conditions of the interior rather than remaining static; i.e., as the pressure and temperature of the planet interior changes, so does the H-He immiscibility curve. Note that, since detailed evolutionary calculations contain metallicity, these miscibility curves were originally calculated using pure H-He mixtures. Therefore, these curves do not account for alterations of the planetary profiles due to metals. Moreover, the H-He EOSes used to calculate the immiscibility curves by SR18 and L0911 differ from those provided here.

4. THERMODYNAMIC CONSISTENCY

The thermodynamic consistency for any EOS requires that its temperature, pressure, and internal energy be in agreement with the first law of thermodynamics, namely

$$T(s, \rho, Y) = \left(\frac{\partial u(s, \rho, Y)}{\partial s} \right)_{\rho, Y} \quad (9)$$

and,

$$P(s, \rho, Y) = \left(\frac{\partial u(s, \rho, Y)}{\partial V} \right)_{s, Y}. \quad (10)$$

In Figure 6, we show regions of thermodynamic space relevant to planetary evolution with shaded regions where each EOS deviates from consistency. The SCvH95 EOS (top row) demonstrates more thermodynamic consistency in important regions for gas giant interiors ($\sim 0.1 \text{ g cm}^{-3}$), showing $\lesssim 2\%$ consistency in these regions. The CMS19+HG23 EOS (bottom row) shows thermodynamic consistency $\lesssim 6\%$ in these regions, in approximate agreement with Becker et al. (2014) in their thermodynamic consistency tests. Thermodynamic inconsistencies imply that energy conservation of planetary evolution models can only be as good as their EOSes allow.

5. GENERALIZED CONVECTION CRITERIA AND THE ENERGY EQUATION

In the standard mixing-length convection theory (Weiss et al. 2004; Kippenhahn et al. 2012; Joyce & Tayar 2023), the associated gedanken thought experiment, a fluid element is displaced and kept isolated at constant pressure with its new surroundings. Isolation in this context means the fluid element maintains a constant entropy and composition. Various structural and thermodynamic derivatives emerge to be important in the context of such theories of convection and convective transport. For simplicity, we evaluate these criteria

assuming that the only compositional variation is in the helium mass fraction, Y , but these expressions can easily be generalized to arbitrarily complex compositional variation. The derivatives in question include (H_P is the pressure scale height):

$$\nabla \equiv \frac{d \log T}{d \log P} \quad (11)$$

$$\nabla_a = \left(\frac{\partial \log T}{\partial \log P} \right)_{s, Y} \quad (12)$$

$$c_P = \left(\frac{\partial s}{\partial \log T} \right)_{P, Y} \quad (13)$$

$$c_V = \left(\frac{\partial s}{\partial \log T} \right)_{\rho, Y} \quad (14)$$

$$\Gamma_1 = \left(\frac{\partial \log P}{\partial \log \rho} \right)_{s, Y} \quad (15)$$

$$\gamma = \left(\frac{\partial \log T}{\partial \log \rho} \right)_{s, Y} \quad (16)$$

$$H_P = - \frac{dr}{d \ln P} \quad (17)$$

$$\chi_T = \left(\frac{\partial \log P}{\partial \log T} \right)_{\rho, Y} \quad (18)$$

$$\chi_\rho = \left(\frac{\partial \log P}{\partial \log \rho} \right)_{T, Y} \quad (19)$$

$$\chi_Y = \left(\frac{\partial \log P}{\partial Y} \right)_{\rho, T} \quad (20)$$

and

$$c_s = \sqrt{\left(\frac{\partial P}{\partial \rho} \right)_{s, Y}}. \quad (21)$$

An exhaustive table of the available values and derivatives for each H-He EOSes is shown in Table 1. Units used in our code are listed in Table 2.

5.1. Convection

The relative density of this isolated fluid compared to that of its surroundings is the criterion for convective stability. In the absence of a composition gradient, the Schwarzschild criterion for convective stability is

$$\nabla - \nabla_a > 0. \quad (22)$$

In the presence of a composition gradient, the Ledoux criterion (Ledoux 1947) for stability must be used instead,

$$\nabla - \nabla_a - B > 0, \quad (23)$$

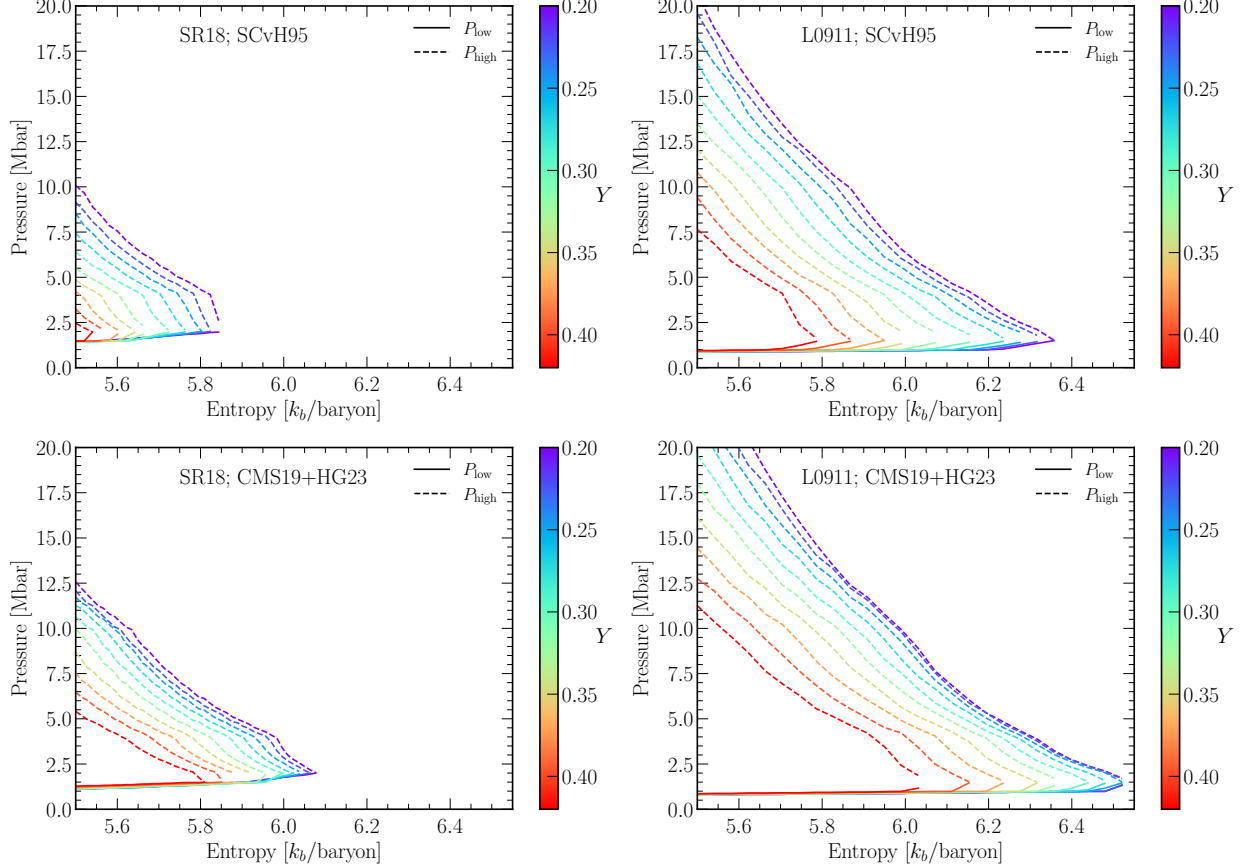


Figure 5. Pressures that enclose the miscibility gap for the L0911 (left column) and SR18 (right column) H-He immiscibility diagrams with the SCvH95 (top row) and CMS19+HG23 (bottom row) EOSes. This figure shows the low and high pressures, marked by solid lines and dashed lines, respectively, where the gap between solid and dashed lines represents the miscibility gap as a function of entropy and helium mass fraction. These high and low pressures are the inner and outer ends of the red lines under the miscibility curve shown in the bottom panel of Figure 4. The low-pressure values are weak functions of helium mass fraction, a behavior also shown in Figure 3. Lower entropies are needed to initiate the immiscibility of H-He at higher helium fractions. Differences in the entropy range are due to the L0911 miscibility curves being hotter than the SR18 curves, allowing immiscibility at higher entropies.

where B is often defined as (Unno et al. 1989)

$$B = -\frac{\chi_Y}{\chi_T} \frac{dY}{d \log P}. \quad (24)$$

The composition gradient term, B , can also be expressed in terms of entropy and composition gradients, derived in Appendix A, as

$$B = \frac{H_P}{c_P} \left[\left(\frac{\partial s}{\partial Y} \right)_{\rho, P} - \left(\frac{\partial s}{\partial Y} \right)_{P, T} \right] \frac{dY}{dr}, \quad (25)$$

where

$$B_1 = \frac{H_P}{c_P} \left(\frac{\partial s}{\partial Y} \right)_{\rho, P} \frac{dY}{dr} \quad (26)$$

$$B_2 = -\frac{H_P}{c_P} \left(\frac{\partial s}{\partial Y} \right)_{P, T} \frac{dY}{dr} \quad (27)$$

such that $B = B_1 + B_2$. The split into B_1 and B_2 is particularly useful. To wit, the superadiabaticity, $\nabla - \nabla_a$, can be shown to be

$$\nabla - \nabla_a = \frac{H_P}{c_P} \frac{ds}{dr} + B_2, \quad (28)$$

so the Schwarzschild criterion for convective stability can then be expressed as

$$\frac{H_P}{c_P} \left[\frac{ds}{dr} - \left(\frac{\partial s}{\partial Y} \right)_{P, T} \frac{dY}{dr} \right] > 0 \quad (29)$$

It is important to note that, in the presence of a composition gradient, marginally Schwarzschild stable regions are not necessarily isentropic. An isentropic structure must meet the criterion

$$\frac{ds}{dr} = 0. \quad (30)$$

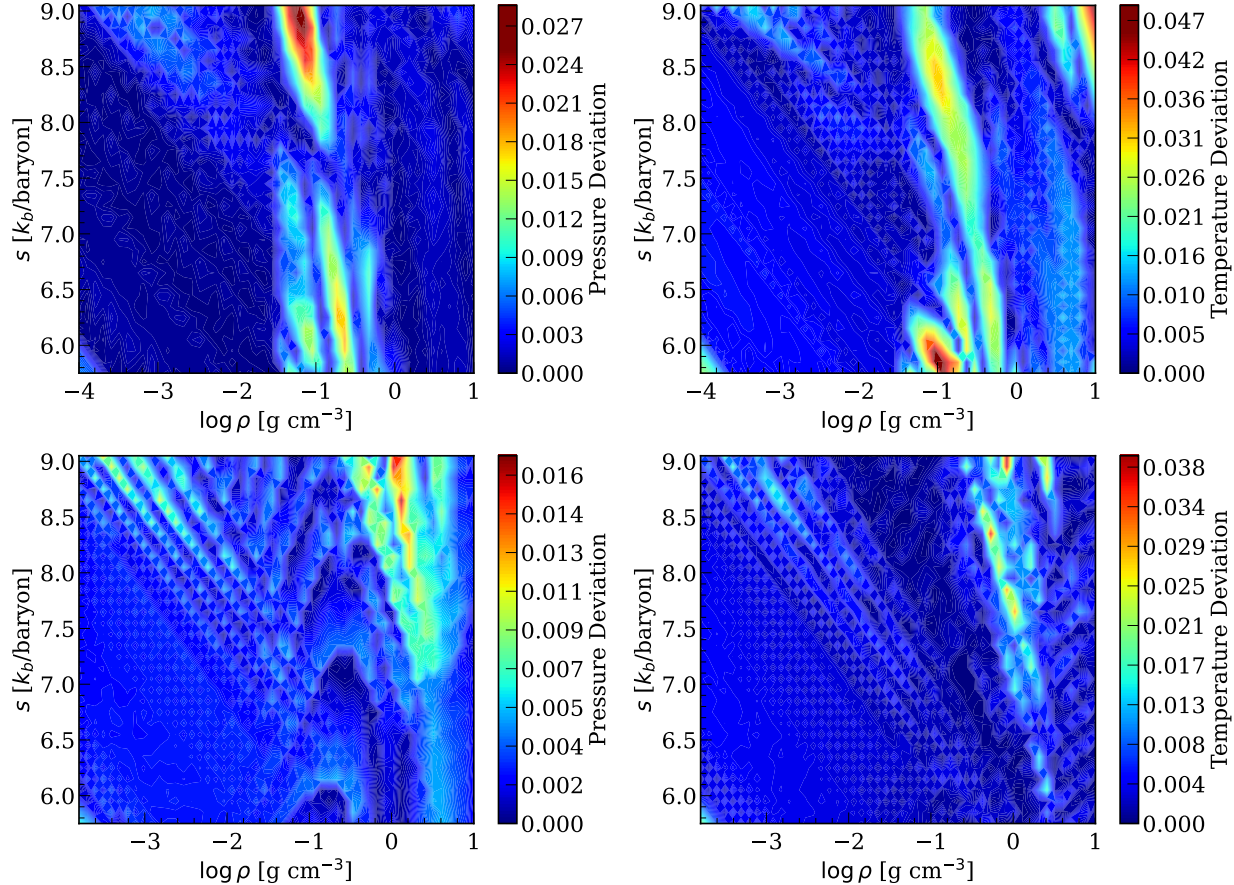


Figure 6. Deviations from thermodynamic consistency indicated by eqs. 9 and 10 for $Y = 0.25$, where zero indicates thermodynamic consistency. The top row shows the thermodynamic consistencies for SCvH95, while the bottom row does so for CMS19+HG23. The SCvH95 EOS appears more thermodynamically consistent than the CMS19+HG23 EOS in H-He density regions most relevant for gas giant interiors ($-2 \leq \log \rho \leq 1$). The highest errors appear at either low entropies with lower densities or high entropies with high densities. In the relevant density regions, the CMS19+HG23 EOS shows $|\text{errors}| \leq 5\%$.

Similarly,

$$\nabla - \nabla_a - B = \frac{H_P}{c_P} \frac{ds}{dr} - B_1, \quad (31)$$

so that the Ledoux criterion for convective stability can be expressed as

$$\frac{H_P}{c_P} \left[\frac{ds}{dr} - \left(\frac{\partial s}{\partial Y} \right)_{\rho, P} \frac{dY}{dr} \right] > 0. \quad (32)$$

In cases where a fluid is stable against convection according to the Ledoux criterion, but Schwarzschild unstable, semiconvection can arise in the form of double diffusive convection (see Walin 1964; Kato 1966; Stevenson 1985; Rosenblum et al. 2011; Leconte & Chabrier 2012; Mirouh et al. 2012; Wood et al. 2013; Leconte & Chabrier 2013; Nettelmann et al. 2015; Moll et al. 2016; Garaud 2018, and references therein). In lieu of any detailed understanding of energy transport in semiconvective regions (Debras et al. 2021b; Mankovich & Fortney 2020; Mankovich et al. 2016; Nettelmann et al. 2015;

Leconte & Chabrier 2012), planetary models have included a density ratio R_0 , which describes the degree to which temperature and composition stratifications contribute to the density stratification to trigger convection. This parameter is defined as (see Rosenblum et al. 2011; Mirouh et al. 2012, for discussions)

$$R_0 = \frac{\nabla - \nabla_a}{\nabla_Y}, \quad (33)$$

where $\nabla_Y = d \log Y / d \log P$ represents the overall composition gradient. Eq. 23 can be written with R_0 as

$$\nabla - \nabla_a - R_0 B > 0. \quad (34)$$

The parameter R_0 can be taken as a free parameter that stretches from 0 (Schwarzschild) to 1 (Ledoux). In terms of entropy, the criterion becomes

Table 1. Repository Quantities and Derivatives for H-He and “metal” EOSes

P, T	ρ, T	s, P	s, ρ
$\log \rho(P, T, Y)$	$\log P(\rho, T, Y)$	$\log \rho(s, P, Y)$	$\log P(s, \rho, Y)$
$s(P, T, Y)$	$s(\rho, T, Y)$	$\log T(s, P, Y)$	$\log T(s, \rho, Y)$
$u(P, T, Y)$	$u(\rho, T, Y)$	$u(s, P, Y)$	$u(s, \rho, Y)$
$(\partial s / \partial Y)_{P,T}$	χ_T	∇_a	c_V
$(\partial \rho / \partial T)_{P,Y}$	χ_ρ	Γ_1	γ
-	χ_Y	c_P	μ_Y
-	$(\partial u / \partial \rho)_{\rho,T}$	c_s	$(\partial u / \partial s)_{s,\rho}$
-	$(\partial s / \partial T)_{\rho,Y}$	$(\partial \rho / \partial s)_{P,Y}$	$(\partial u / \partial \rho)_{s,Y}$
-	$(\partial s / \partial Y)_{\rho,T}$	$(\partial T / \partial Y)_{s,P}$	$(\partial T / \partial Y)_{s,\rho}$
-	-	-	$(\partial T / \partial s)_{\rho,Y}$
-	-	-	$(\partial T / \partial \rho)_{s,Y}$
-	-	-	$(\partial s / \partial Y)_{\rho,P}$

NOTE—These quantities and derivatives are also available as a function of Z . The logarithmic quantities are log base 10, and the units are tabulated in Table 2. The original CMS19 tables were provided by their authors in the bases (P, T) and (ρ, T) . To ensure consistency, we used the original pressure-temperature combined with the HG23 components to obtain new ρ, T tables. All quantities and derivatives of the CMS19 and MLS22 tables contain these non-ideal corrections. The thermodynamic quantities and derivatives are also available for pure water (AQUA), post-perovskite, serpentine, and iron, along with the provided “metal” mixture tables.

$$\underbrace{\frac{ds}{dr} - \left\{ \left(\frac{\partial s}{\partial Y} \right)_{P,T} + R_0 \left[\underbrace{\left(\frac{\partial s}{\partial Y} \right)_{P,T} - \left(\frac{\partial s}{\partial Y} \right)_{\rho,P}} \right] \right\} \frac{dY}{dr}}_{(35)}.$$

$$= \frac{c_P}{H_P} (\nabla - \nabla_a) = \frac{c_P}{H_P} (B_1 + B_2)$$

If $R_\rho = 0$, then Eq. 35 reduces to the Schwarzschild criterion, Eq. 29. If $R_\rho = 1$, then Eq. 35 reduces to the Ledoux criterion, Eq. 32, modulo the c_P/H_P factor.

In the repository, we provide these derivatives in functional and tabulated form, with the choice of parameter R_0 . Figure 7 shows the sign changes of the relevant derivatives for the convection criteria at typical values in the interior of gas giants. A negative $(\partial s / \partial Y)_{P,T}$ ensures that when the Schwarzschild convection stability condition is violated (i.e., convection occurs), the resulting entropy gradient is positive, assuming that the composition gradient (dY/dr) is negative. This would also hold for the Ledoux condition against convection but for $(\partial s / \partial Y)_{\rho,P}$. The sign change of this derivative at interior conditions indicates that the reverse occurs; namely, the entropy profile gradient becomes negative

Table 2. Standard Units

Quantity	Units
s (independent)	k_b/baryon
s (dependent)	$\text{erg g}^{-1} \text{K}^{-1}$
$\log \rho$	g cm^{-3}
$\log P$	dyn cm^{-2}
$\log T$	K
$\log u$	erg g^{-1}

NOTE—Standard units used throughout our EOS module. The EOS module provides thermodynamic quantities as a function of entropy; the independent entropy is expressed in units of k_b/baryon . If entropy is the dependent variable, our code will output the entropy in cgs units. We do not provide the internal energy as an independent variable.

when the Ledoux convection stability condition is violated in these regions.

We also provide the expressions to compute the Brunt-Väisälä frequency (N), which is the buoyant oscillation frequency in a stable stratified fluid. This frequency is defined as (Lattimer & Mazurek 1981; Unno et al. 1989; Saio 1993; Passamonti et al. 2009; Fuller et al. 2016; Mankovich & Fuller 2021, also shown in Appendix B.):

$$N^2 = g^2 \left[\frac{d\rho}{dP} - \left(\frac{\partial \rho}{\partial P} \right)_{s,Y} \right], \quad (36)$$

which can be shown³ to be equal to

$$N^2 = \frac{g}{c_P} \frac{\chi_T}{\chi_\rho} \left[\frac{ds}{dr} - \left(\frac{\partial s}{\partial Y} \right)_{\rho,P} \frac{dY}{dr} \right]. \quad (37)$$

5.2. The energy equation

The thermodynamic energy equation can be given by the first law of thermodynamics. If rendered in the independent thermodynamic basis variables ($s, \rho = \frac{1}{V}, N_j$), this yields

$$dU + PdV = Tds + \sum_{j=1}^n \mu_j dN_j \quad (38)$$

for n chemical components. It is the left-hand-side of this equation that appears in the energy equation in stel-

³ in Appendix B

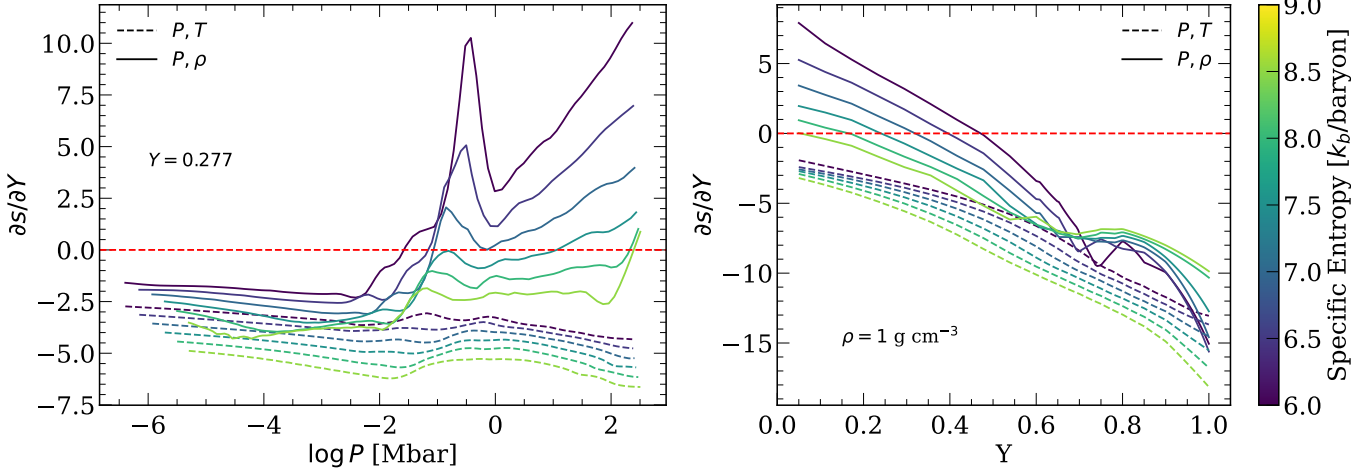


Figure 7. Entropy-composition derivatives as a function of pressure (left) and helium mass fraction (right), at constant (P, T) (dashed line) and constant (ρ, P) (solid line). The red dashed line indicates the sign change. In particular, the derivative relevant to the Ledoux condition, $(\partial s / \partial Y)_{\rho, P}$, changes sign from negative to positive in the interior as a function of pressure, and at moderate to low helium abundances ($\lesssim 0.40$) for a typical density and entropy in the interior H-He envelope of Jupiter.

lar/planetary evolution and that is related to the energy sources, sinks, and the divergence of the energy flux. If the thermodynamic basis variables are (ρ, T, N_j) , then a knowledge of $U(\rho, T, N_j)$ allows one to eschew explicit mention of s .

However, if we employ the entropy formulation and include only the dependence upon Y (the helium mass fraction), the specific energy (energy per mass) can be written as

$$du + Pd\left(\frac{1}{\rho}\right) = Tds + \mu_Y dY. \quad (39)$$

We note that μ_Y is not the helium chemical potential but the weighted sum emerging from the right-hand side of Eq. 39. This can be easily expanded to include metals (Z) specifically by adding a $\mu_Z dZ$ term, but is in fact already implicit in Eq. 39. The composition then is included in the energy update when using entropy as an independent variable for a given evolutionary calculation step. Following Eq. 39, the term μ_Y for the hydrogen-helium mixture is

$$\mu_Y = \left(\frac{\partial u}{\partial Y} \right)_{s, \rho}. \quad (40)$$

Recent giant planet evolutionary calculations, such as those of Mankovich et al. (2016), and Mankovich & Fortney (2020), have approximated this term by differentiating the energy throughout the resolution of the profile (see Section 2.5 of Mankovich et al. 2016). Stellar evolution codes such as MESA (Paxton et al. 2011) have recently updated their fundamental energy equations to include explicitly the chemical potential (see Section 8 of Paxton et al. 2018). Along with the tables provided

with this article, we also provide a means of obtaining this term for any S, ρ, Y , regardless of the interior profile.

6. CONCLUSION

With this paper, and its associated website (https://github.com/Rob685/hhe_eos_misc), we provide a more centralized and organized way to access the crucial hydrogen-helium mixture equations of state, accompanied by the various derivatives necessary to calculate heat transport and different convection criteria. The EOSes and derivatives are recalculated in the range $-6 \leq \log_{10} P \leq 2$ Mbar and $2 \leq \log_{10} T \leq 5$ Kelvin, a range that is comparable to each of the EOS tables that we have adapted. This work allows for the prompt calculation of the derivatives required in the convection criteria for stability, namely, the partial derivatives in Eqs. 35 and 37. Importantly, we calculate the pseudo-chemical potential (Eq. 40) so that it is readily available for energy calculations for any helium mixture.

Furthermore, we make the miscibility curves from L0911 and SR18 accessible to the community of planetary modelers. As discussed in Section 3.3, we provide the ability to calculate the miscibility curves for general planetary profiles without restricting to a single value of Y . The present work marks a step toward addressing the many inconsistencies between EOSes, miscibility curves, and other physics relevant to planetary evolution. Important future work by the community includes the calculation of self-consistent H-He immiscibility and EOS curves that incorporate all nonideal interactions between H-He and metals in a self-consistent fashion. Such a future project will remove many of the remaining

ambiguities in the thermodynamics of the giant planets of our solar system and beyond.

APPENDIX

A. COMPOSITION GRADIENT TERM WITH ENTROPY GRADIENTS

Recall that with a composition gradient the criterion for stability against convection is Eq. 23. Using the definition in Eq. 24,

$$\nabla - \nabla_a - \left(\frac{\partial \log T}{\partial Y} \right)_{\rho, P} \frac{dY}{d \log P} > 0. \quad (\text{A1})$$

Recognizing that

$$\left(\frac{\partial \log T}{\partial Y} \right)_{\rho, P} = \left(\frac{\partial \log T}{\partial Y} \right)_{s, P} + \left(\frac{\partial \log T}{\partial s} \right)_{P, Y} \left(\frac{\partial s}{\partial Y} \right)_{\rho, P}, \quad (\text{A2})$$

B in Eq. 24 can be written in terms of two derivatives of the entropy with respect to the helium mass fraction Y ,

$$\begin{aligned} B &= \left(\frac{\partial \log T}{\partial s} \right)_{P, Y} \left[\left(\frac{\partial s}{\partial Y} \right)_{\rho, P} - \left(\frac{\partial s}{\partial Y} \right)_{P, T} \right] \frac{dY}{d \log P}. \\ &= \frac{P}{c_P} \left[\left(\frac{\partial s}{\partial Y} \right)_{\rho, P} - \left(\frac{\partial s}{\partial Y} \right)_{P, T} \right] \frac{dY}{dP} \end{aligned} \quad (\text{A3})$$

where the two terms can be assigned the names B_1 and B_2 ,

$$B_1 = \frac{P}{c_P} \left(\frac{\partial s}{\partial Y} \right)_{\rho, P} \frac{dY}{dP}, \quad (\text{A4})$$

$$B_2 = -\frac{P}{c_P} \left(\frac{\partial s}{\partial Y} \right)_{P, T} \frac{dY}{dP} \quad (\text{A5})$$

such that $B = B_1 + B_2$ and as discussed in §5. Using the pressure scale height, these terms can be written in terms of entropy and composition profile gradients,

$$B_1 = -\frac{H_P}{c_P} \left(\frac{\partial s}{\partial Y} \right)_{\rho, P} \frac{dY}{dr} \quad (\text{A6})$$

$$B_2 = \frac{H_P}{c_P} \left(\frac{\partial s}{\partial Y} \right)_{P, T} \frac{dY}{dr}. \quad (\text{A7})$$

B. THE BRUNT VÄISÄLÄ FREQUENCY IN TERMS OF ENTROPY AND COMPOSITION

Let $\rho = \rho(S, P, Y)$ so that

$$d \log \rho = \left(\frac{\partial \log \rho}{\partial \log P} \right)_{s, Y} d \log P + \left(\frac{\partial \log \rho}{\partial s} \right)_{P, Y} ds + \left(\frac{\partial \log \rho}{\partial Y} \right)_{P, s} dY, \quad (\text{B8})$$

implying that

$$\frac{d \log \rho}{d \log P} = \left(\frac{\partial \log \rho}{\partial \log P} \right)_{s, Y} + \left(\frac{\partial \log \rho}{\partial s} \right)_{P, Y} \frac{ds}{d \log P} + \left(\frac{\partial \log \rho}{\partial Y} \right)_{P, s} \frac{dY}{d \log P}. \quad (\text{B9})$$

Using the relation on the right-hand side of Eq. 36,

$$N^2 = \frac{\rho g^2}{P} \left[\left(\frac{\partial \log \rho}{\partial s} \right)_{P, Y} \frac{ds}{d \log P} + \left(\frac{\partial \log \rho}{\partial Y} \right)_{s, P} \frac{dY}{d \log P} \right], \quad (\text{B10})$$

which becomes

$$N^2 = \frac{\rho g^2}{P} \left(\frac{\partial \log \rho}{\partial s} \right)_{P,Y} \left[\frac{ds}{d \log P} - \left(\frac{\partial s}{\partial \log Y} \right)_{\rho,P} \frac{dY}{d \log P} \right]. \quad (\text{B11})$$

Using

$$g^2 = -\frac{gP}{\rho} \frac{d \log P}{dr},$$

and converting to non-logarithmic derivatives, this becomes

$$N^2 = -\frac{g}{\rho} \left(\frac{\partial \rho}{\partial s} \right)_{P,Y} \left[\frac{ds}{dr} - \left(\frac{\partial s}{\partial Y} \right)_{\rho,P} \frac{dY}{dr} \right], \quad (\text{B12})$$

which is the expression found in [Lattimer & Mazurek \(1981\)](#). Using the relation

$$\left(\frac{\partial \rho}{\partial s} \right)_{P,Y} = -\frac{\chi_T}{\chi_\rho} \frac{\rho}{c_P}, \quad (\text{B13})$$

the Brunt Väisälä frequency (squared) can now be written as

$$N^2 = \frac{g}{c_P} \frac{\chi_T}{\chi_\rho} \left[\frac{ds}{dr} - \left(\frac{\partial s}{\partial Y} \right)_{\rho,P} \frac{dY}{dr} \right]. \quad (\text{B14})$$

¹ Funding (or partial funding) for this research was provided by the Center for Matter at Atomic Pressures (CMAP),
² a National Science Foundation (NSF) Physics Frontier Center, under Award PHY-2020249. Any opinions, findings,
³ conclusions or recommendations expressed in this material are those of the author(s) and do not necessarily reflect
⁴ those of the National Science Foundation. YS is supported by a Lyman Spitzer, Jr. Postdoctoral Fellowship at
⁵ Princeton University.

REFERENCES

Baraffe, I., Chabrier, G., Allard, F., & Hauschildt, P. H. 1998, *A&A*, 337, 403. <https://articles.adsabs.harvard.edu/pdf/1998A%26A...337..403B>

Becker, A., Lorenzen, W., Fortney, J. J., et al. 2014, *The Astrophysical Journal Supplement Series*, 215, 21, doi: [10.1088/0067-0049/215/2/21](https://doi.org/10.1088/0067-0049/215/2/21)

Becker, A., Nettelmann, N., Holst, B., & Redmer, R. 2013, *PHYSICAL REVIEW B*, 88, 45122, doi: [10.1103/PhysRevB.88.045122](https://doi.org/10.1103/PhysRevB.88.045122)

Bolton, S. J., Lunine, J., Stevenson, D., et al. 2017a, *Space Science Reviews*, 213, 5, doi: [10.1007/s11214-017-0429-6](https://doi.org/10.1007/s11214-017-0429-6)

Bolton, S. J., Adriani, A., Adumitroaie, V., et al. 2017b, *Science*, 356, 821, doi: [10.1126/SCIENCE.AAL2108](https://doi.org/10.1126/SCIENCE.AAL2108)

Bryggo, S., Loubeyre, P., Millot, M., et al. 2021, *Nature*, 593, doi: [10.1038/s41586-021-03516-0](https://doi.org/10.1038/s41586-021-03516-0)

Burrows, A. 2014, *Proceedings of the National Academy of Sciences*, 111, doi: [10.1073/pnas.1304208111/-/DCSupplemental](https://doi.org/10.1073/pnas.1304208111/-/DCSupplemental)

Burrows, A., Hubbard, W. B., Lunine, J. I., & Liebert, J. 2001, *Reviews of Modern Physics*, 73. <https://journals.aps.org/rmp/pdf/10.1103/RevModPhys.73.719>

Burrows, A., Saumon, D., Guillot, T., Hubbard, W., & Luninet, J. I. 1995, *Letters to Nature*, 375, 299. <https://www.nature.com/articles/375299a0>

Burrows, A., Marley, M., Hubbard, W., et al. 1997, *ApJ*, 491, 856. <https://iopscience.iop.org/article/10.1086/305002/pdf>

Caillabet, L., Mazeved, S., & Loubeyre, P. 2011, *Physical Review B*, 83, 94101, doi: [10.1103/PhysRevB.83.094101](https://doi.org/10.1103/PhysRevB.83.094101)

Chabrier, G., & Baraffe, I. 1997, *A&A*, 327, 1039. <https://articles.adsabs.harvard.edu/pdf/1997A%26A...327.1039C>

Chabrier, G., & Debras, F. 2021, *ApJ*, 917, 6pp, doi: [10.3847/1538-4357/abfc48](https://doi.org/10.3847/1538-4357/abfc48)

Chabrier, G., Mazeved, S., & Soubiran, F. 2019, *ApJ*, 872, 27pp, doi: [10.3847/1538-4357/aaf99f](https://doi.org/10.3847/1538-4357/aaf99f)

Chabrier, G., & Potekhin, A. Y. 1998, *Physical Review E*, 58. <https://journals.aps.org/pre/pdf/10.1103/PhysRevE.58.4941>

Chen, Y.-X., Burrows, A., Sur, A., & Arevalo, R. T. 2023, *ApJ*, 957, 8, doi: [10.3847/1538-4357/acf456](https://doi.org/10.3847/1538-4357/acf456)

Debras, F., & Chabrier, G. 2019, *ApJ*, 872, 22pp, doi: [10.3847/1538-4357/aaff65](https://doi.org/10.3847/1538-4357/aaff65)

Debras, F., Chabrier, G., & Stevenson, D. J. 2021a, *The Astrophysical Journal Letters*, 913, 7pp, doi: [10.3847/2041-8213/abfdcc](https://doi.org/10.3847/2041-8213/abfdcc)

—. 2021b, *The Astrophysical Journal Letters*, 913, L21, doi: [10.3847/2041-8213/abfdcc](https://doi.org/10.3847/2041-8213/abfdcc)

Folkner, W. M., Iess, L., Anderson, J. D., et al. 2017, *Geophysical Research Letters*, 44, 4694, doi: [10.1002/2017GL073140](https://doi.org/10.1002/2017GL073140)

Fortney, J. J., & Hubbard, W. B. 2003, *Icarus*, 164, 228, doi: [10.1016/S0019-1035\(03\)00130-1](https://doi.org/10.1016/S0019-1035(03)00130-1)

—. 2004, *ApJ*, 608, 1039

Fortney, J. J., Ikoma, M., Nettelmann, N., Guillot, T., & Marley, M. S. 2011, *The Astrophysical Journal*, 729, 32, doi: [10.1088/0004-637X/729/1/32](https://doi.org/10.1088/0004-637X/729/1/32)

Fuller, J., Luan, J., & Quataert, E. 2016, *MNRAS*, 458, 3867, doi: [10.1093/mnras/stw609](https://doi.org/10.1093/mnras/stw609)

Garaud, P. 2018, *Annu. Rev. Fluid Mech.*, 50, 275, doi: [10.1146/annurev-fluid-122316](https://doi.org/10.1146/annurev-fluid-122316)

Guillot, T., Burrows, A., Hubbard, W. B., Lunine, J. I., & Saumon, D. 1996, *ApJ*, 459, 35. <https://iopscience.iop.org/article/10.1086/309935/pdf>

Helled, R., Stevenson, D. J., Lunine, J. I., et al. 2022, *Icarus*, 378, 114937, doi: [10.1016/j.icarus.2022.114937](https://doi.org/10.1016/j.icarus.2022.114937)

Howard, S., & Guillot, T. 2023, *A&A*, 672, doi: [10.5281/zenodo](https://doi.org/10.5281/zenodo)

Howard, S., Guillot, T., Bazot, M., et al. 2023, *A&A*, doi: [10.5281/zenodo.7598377](https://doi.org/10.5281/zenodo.7598377)

Hubbard, W. 1970, *ApJ*, 162. <https://articles.adsabs.harvard.edu/pdf/1970ApJ...162..687H>

Hubbard, W. B., & Dewitt, H. E. 1985, *The Astrophysical Journal*, 290, 388. https://articles.adsabs.harvard.edu/cgi-bin/nph-iarticle_query?1985ApJ...290..388H&defaultprint=YES&filetype=.pdf

Hubbard, W. B., & Militzer, B. 2016, *The Astrophysical Journal*, 820, 13pp, doi: [10.3847/0004-637X/820/1/80](https://doi.org/10.3847/0004-637X/820/1/80)

Hubbard, W. B., & Slattery, W. L. 1971, *The Astrophysical Journal*, 168, 131, doi: [10.1086/151068](https://doi.org/10.1086/151068)

Joyce, M., & Tayar, J. 2023, *MDPI*. <https://arxiv.org/pdf/2303.09596.pdf>

Kato, S. 1966, *Publications of the Astronomical Society of Japan*, 18

Kippenhahn, R., Weigert, A., & Weiss, A. 2012, *Stellar Structure & Evolution*, 2nd edn. (New York: Springer)

Lattimer, J. M., & Mazurek, T. J. 1981, *ApJ*, 246, 955

Leconte, J., & Chabrier, G. 2012, *A&A*, 540, 20, doi: [10.1051/0004-6361/201117595](https://doi.org/10.1051/0004-6361/201117595)

—. 2013, *Nature Geoscience*, doi: [10.1038/NGEO1791](https://doi.org/10.1038/NGEO1791)

Ledoux, P. 1947, *ApJ*, 105

Lorenzen, W., Holst, B., & Redmer, R. 2009, *Physical Review Letters*, 102, doi: [10.1103/PhysRevLett.102.115701](https://doi.org/10.1103/PhysRevLett.102.115701)

—. 2011, *Physical Review B*, 84, doi: [10.1103/PhysRevB.84.235109](https://doi.org/10.1103/PhysRevB.84.235109)

Mankovich, C., Fortney, J. J., & Moore, K. L. 2016, *ApJ*, 832, 13pp, doi: [10.3847/0004-637X/832/2/113](https://doi.org/10.3847/0004-637X/832/2/113)

Mankovich, C. R., & Fortney, J. J. 2020, *The Astrophysical Journal*, 889, 51, doi: [10.3847/1538-4357/ab6210](https://doi.org/10.3847/1538-4357/ab6210)

Mankovich, C. R., & Fuller, J. 2021, *Nature Astronomy*, 5, 1103, doi: [10.1038/s41550-021-01448-3](https://doi.org/10.1038/s41550-021-01448-3)

Mazevet, S., Licari, A., & Soubiran, F. 2022, *Astronomy & Astrophysics*, 664, A112, doi: [10.1051/0004-6361/201935764](https://doi.org/10.1051/0004-6361/201935764)

Miguel, Y., Guillot, T., & Fayon, L. 2016, *A&A*, 596, doi: [10.1051/0004-6361/201629732](https://doi.org/10.1051/0004-6361/201629732)

Miguel, Y., Bazot, M., Guillot, T., et al. 2022, *A&A*, 662, doi: [10.1051/0004-6361/202243207](https://doi.org/10.1051/0004-6361/202243207)

Militzer, B. 2009, *Physical Review B*, 79. <https://journals.aps.org/prb/pdf/10.1103/PhysRevB.79.155105>

Militzer, B., & Hubbard, W. B. 2013, *The Astrophysical Journal*, 774, 148, doi: [10.1088/0004-637X/774/2/148](https://doi.org/10.1088/0004-637X/774/2/148)

Militzer, B., Hubbard, W. B., Vorberger, J., Tamblyn, I., & Bonev, S. A. 2008, *The Astrophysical Journal*, 688, 45. <https://iopscience.iop.org/article/10.1086/594364/pdf>

Militzer, B., Hubbard, W. B., Wahl, S., et al. 2022, *The Planetary Science Journal*, 3, 185, doi: [10.3847/PSJ/ac7ec8](https://doi.org/10.3847/PSJ/ac7ec8)

Mirouh, G. M., Garaud, P., Stellmach, S., Traxler, A. L., & Wood, T. S. 2012, *The Astrophysical Journal*, 750, 61, doi: [10.1088/0004-637X/750/1/61](https://doi.org/10.1088/0004-637X/750/1/61)

Moll, R., Garaud, P., & Stellmach, S. 2016, *The Astrophysical Journal*, 823, doi: [10.3847/0004-637X/823/1/33](https://doi.org/10.3847/0004-637X/823/1/33)

Morales, M. A., Hamel, S., Caspersen, K., & Schwegler, E. 2013, *Physical Review B*, 87, 174105, doi: [10.1103/PhysRevB.87.174105](https://doi.org/10.1103/PhysRevB.87.174105)

Morales, M. A., Schwegler, E., Ceperley, D., et al. 2009, *Proceedings of the National Academy of Sciences of the United States of America*, 106, 1324, doi: [10.1073/pnas.0812581106](https://doi.org/10.1073/pnas.0812581106)

Myers, W. D., & Swiatecki, W. J. 1990, *Annals of Physics*, 204, 401, doi: [10.1016/0003-4916\(90\)90395-5](https://doi.org/10.1016/0003-4916(90)90395-5)

—. 1996, *Nuclear Physics A*, 601, 141, doi: [10.1016/0375-9474\(95\)00509-9](https://doi.org/10.1016/0375-9474(95)00509-9)

Nettelmann, N., Becker, A., & Redmer, R. 2012, *The Astrophysical Journal*, 750, 52, doi: [10.1088/0004-637X/750/1/52](https://doi.org/10.1088/0004-637X/750/1/52)

Nettelmann, N., Fortney, J. J., Moore, K., & Mankovich, C. 2015, MNRAS, 447, 3422, doi: [10.1093/mnras/stu2634](https://doi.org/10.1093/mnras/stu2634)

Nettelmann, N., Holst, B., Kietzmann, A., et al. 2008, ApJ, 683, 1217

Passamonti, A., Haskell, B., Andersson, N., Jones, D. I., & Hawke, I. 2009, Mon. Not. R. Astron. Soc, 394, 730, doi: [10.1111/j.1365-2966.2009.14408.x](https://doi.org/10.1111/j.1365-2966.2009.14408.x)

Paxton, B., Bildsten, L., Dotter, A., et al. 2011, The Astrophysical Journal Supplement Series, 192, 3, doi: [10.1088/0067-0049/192/1/3](https://doi.org/10.1088/0067-0049/192/1/3)

Paxton, B., Schwab, J., Bauer, E. B., et al. 2018, ApJ, 234, 50pp, doi: [10.3847/1538-4365/aaa5a8](https://doi.org/10.3847/1538-4365/aaa5a8)

Perdew, J. P., Burke, K., & Ernzerhof, M. 1996, Physical Review letters, 77. <https://doi.org/10.1103/PhysRevLett.77.3865>

Pfaffenzeller, O., Hohl, D., & Ballone, P. 1995, Physical Review Letters, 74

Pollack, J. B., & Grabske, H. C. 1976, Icarus, 29, 35. <https://doi.org/10.1016/0019103576901007>

Pollack, J. B., Grossman, A. S., Moore, R., & Grabske, H. C. 1977, Icarus, 30, 111, doi: [10.1016/0019-1035\(77\)90126-9](https://doi.org/10.1016/0019-1035(77)90126-9)

Püstow, R., Nettelmann, N., Lorenzen, W., & Redmer, R. 2016, Icarus, 267, 323, doi: [10.1016/j.icarus.2015.12.009](https://doi.org/10.1016/j.icarus.2015.12.009)

Rogers, F. J. 1981, Physical Review A, 24, 1531, doi: [10.1103/PhysRevA.24.1531](https://doi.org/10.1103/PhysRevA.24.1531)

Rogers, F. J., & Young, D. A. 1984, Physical Review A, 30. <https://doi.org/10.1103/PhysRevA.30.999>

Rosenblum, E., Garaud, P., Traxler, A., & Stellmach, S. 2011, The Astrophysical Journal, 731, 66, doi: [10.1088/0004-637X/731/1/66](https://doi.org/10.1088/0004-637X/731/1/66)

Saio, H. 1993, Astrophysics and Space Science, 210, 61. [https://doi.org/10.1007/BF00657873.pdf](https://doi.org/10.1007/BF00657873)

Saumon, D., Chabrier, G., & Van Horn, H. M. 1995, The Astrophysical Journal Supplement Series, 99, 713

Saumon, D., Hubbard, W. B., Burrows, A., et al. 1996, ApJ. <https://doi.org/10.1088/0004-637X/460/2/993>

Schöttler, M., & Redmer, R. 2018, Physical Review Letters, 120, doi: [10.1103/PhysRevLett.120.115703](https://doi.org/10.1103/PhysRevLett.120.115703)

Schouten, J. A., De Kuijper, A., & Michels, J. P. J. 1991, PHYSICAL REVIEW, 8. <https://doi.org/10.1103/PhysRevB.44.6630>

Seiff, A., Kirk, D. B., Knight, T. C., et al. 1997, Science, 276, 102, doi: [10.1126/science.276.5309.102](https://doi.org/10.1126/science.276.5309.102)

—. 1998, Journal of Geophysical Research: Planets, 103, 22857, doi: [10.1029/98JE01766](https://doi.org/10.1029/98JE01766)

Stevenson, D. J. 1975, Physical Review B, 12. <https://doi.org/10.1103/PhysRevB.12.3999>

—. 1985, Icarus, 62, 4

—. 2020, Annual Review of Earth and Planetary Sciences, 48, 465, doi: [10.1146/annurev-earth-081619-052855](https://doi.org/10.1146/annurev-earth-081619-052855)

Stevenson, D. J., & Salpeter, E. E. 1977, The Astrophysical Journal Supplement Series, 35, 221. <https://doi.org/10.1088/0067-0049/35/2/221>

Unno, W., Osaki, Y., Ando, H., & Shibahashi, H. 1989, Nonradial oscillations of stars, 2nd edn. (Tokyo: Tokyo University Press)

Vazan, A., Helled, R., & Guillot, T. 2018, A&A, 610, 14, doi: [10.1051/0004-6361/201732522](https://doi.org/10.1051/0004-6361/201732522)

Vazan, A., Helled, R., Podolak, M., & Kovetz, A. 2016, ApJ, 829, doi: [10.3847/0004-637X/829/2/118](https://doi.org/10.3847/0004-637X/829/2/118)

Wahl, S. M., Hubbard, W. B., Militzer, B., et al. 2017, Geophysical Research Letters, 44, 4649, doi: [10.1002/2017GL073160](https://doi.org/10.1002/2017GL073160)

Walin, G. 1964, Tellus, 16, 389, doi: [10.1111/J.2153-3490.1964.TB00175.X](https://doi.org/10.1111/J.2153-3490.1964.TB00175.X)

Weiss, A., Hillebrandt, W., Thomas, H., & Ritter, H. 2004, Cox and Giuli's Principles of Stellar Structure, 2nd edn. (Cambridge, UK: Cambridge Scientific Publishers Ltd)

Wood, T. S., Garaud, P., & Stellmach, S. 2013, The Astrophysical Journal, 768, 157, doi: [10.1088/0004-637X/768/2/157](https://doi.org/10.1088/0004-637X/768/2/157)